Adiabatic study of the positronium negative ion

Javier Botero*
Department of Physics and Astronomy, Louisiana State University, Baton Rouge, Louisiana 70803
(Received 19 August 1986)

The positronium negative ion is studied using an adiabatic treatment in hyperspherical coordinates. The potential curves of five different symmetries, $^1S^e$, $^1P^o$, $^3P^o$, $^3P^e$, and $^1D^e$, are discussed along with the corresponding resonant states. A new method for calculating the body-frame probability density is used to study the different symmetries and to distinguish between them.

I. INTRODUCTION

The recent advances in experimental techniques for studying systems containing positrons have brought much interest to their theoretical study. Among these, there is particular interest in the positronium negative ion (Ps^- throughout this paper), a three-particle system (one positron and two electrons) whose existence was first predicted by Wheeler[1] and recently confirmed experimentally by Mills,[2] who also measured its lifetime.[3] Ps^- is a simple system which can bring much information about the dependence of the dynamics of three-bound-particle systems on the relative masses of the particles.[4] It is well known[5–6] that there is a simple relationship between the Ps^- and H^- ground-state total energy, between the ground-state binding energies, and between the binding energies of the lowest $^1S^e$ doubly excited resonances. In each case the Ps^- values are approximately one-half of the corresponding energies in H^-. It has also been predicted[7] that the photodetachment cross section of Ps^- parallels that of H^-. The dominant resonance features in H^-, a single + shape resonance and an infinite series of − Feshbach resonances, have also been predicted in Ps^- $^1P^o$.[7] A question then arises: does this scaling factor hold for all different symmetries? Or, more generally, is there a resemblance throughout the whole spectrum of these two systems? In an attempt to answer this question I present here the results of a study of five different symmetries of Ps^-, namely $^1S^e$, $^1P^o$, $^3P^e$, $^3P^o$, and $^1D^e$, using an adiabatic treatment in hyperspherical coordinates. A prediagonalized basis of hyperspherical harmonics[7] is used as basis for the expansion of the adiabatic function. In order to study the characteristic properties of the different symmetries and to distinguish among them, I present a method for calculating the body-frame probability density.[8] This will also corroborate the diabatic interpolation of the + and − potential curves made in Ref. 7 (hereafter called BG).

Section II of this paper presents the problem and the coordinate system to be used. Section III reviews briefly the hyperspherical coordinates and the adiabatic treatment. Section IV describes the solution of the adiabatic eigenvalue equation for arbitrary total angular momentum using hyperspherical harmonics as basis functions. Section V discusses the results and Sec. VI consists of some concluding remarks. The computation of the matrix elements $U_{ml_1l_2m'l_1'l_2'}$ is described in Appendix A and the calculation of the body-frame probability density is presented in Appendix B.

II. THE COORDINATE SYSTEM AND THE SCHRÖDINGER EQUATION

Different coordinate systems have been used to describe three-particle systems depending mainly on the relative masses of the particles. For two-electron atoms, independent-particle-type coordinates $(\mathbf{r}_1,\mathbf{r}_2)$ are usually used, where $\mathbf{r}_1$ represents the position vector of electron 1 relative to the nucleus, and $\mathbf{r}_2$ represents that of electron 2. The full Hamiltonian in these coordinates is

$$H=-\frac{1}{2\mu}\nabla_1^2-\frac{1}{2\mu}\nabla_2^2-\frac{m}{M}\nabla_1\cdot\nabla_2-\frac{Z}{r_1}-\frac{Z}{r_2}+\frac{1}{r_{12}}\ , \quad (1)$$

where μ is the reduced mass of the electron-nucleus pair, m is the mass of the electron, M is the mass of the nucleus, and Z is the nuclear charge. In the usual case of a heavy nucleus m/M is small, and this term may be neglected or treated in perturbation theory.[9]

When the three particles are of comparable masses, as is the case in Ps^-, the cross term $\nabla_1\cdot\nabla_2$ is as important as the other two terms of the kinetic energy operator and cannot be treated perturbatively. In order to avoid the complications involved with this term, I describe the three-particle configuration space in terms of symmetric Jacobi coordinates $(\mathbf{r}_1,\mathbf{x})$ defined as follows:

$$\begin{aligned}\mathbf{r}_1&=\mathbf{r}_{m_2}-\mathbf{r}_{m_1}\ ,\\ \mathbf{x}&=-\tfrac{1}{2}(\mathbf{r}_{m_1}+\mathbf{r}_{m_2})+\mathbf{r}_{m_3}\ ,\end{aligned} \quad (2)$$

where $\mathbf{r}_{m_1}$, $\mathbf{r}_{m_2}$, and $\mathbf{r}_{m_2}$ are the position vectors of particles 1, 2, and 3, respectively (see Fig. 1), relative to the center of mass of the system.

The Hamiltonian in these coordinates is

$$H=T+V\ , \quad (3)$$

where

$$\begin{aligned}T&=-\frac{1}{2m_1}\nabla_{m_1}^2-\frac{1}{2m_2}\nabla_{m_2}^2-\frac{1}{2m_3}\nabla_{m_3}^2\ ,\\ T&=-\frac{1}{2\mu_{12}}\nabla_{r_1}^2-\frac{1}{2\mu_{12,3}}\nabla_x^2\ ,\end{aligned} \quad (4)$$

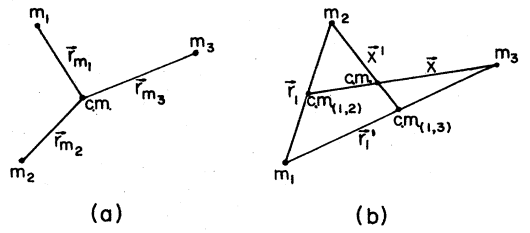

FIG. 1. Coordinate systems used to describe three-particle systems in their center-of-mass frame. (a) shows the independent-particle coordinates and (b) shows the Jacobi coordinates $(\mathbf{r}_1,\mathbf{x})$ and $(\mathbf{r}_1,\mathbf{x}')$ used in the present study.

and

$$V=\frac{1}{|\mathbf{r}_1|}-\frac{1}{|\frac{1}{2}\mathbf{r}_1+\mathbf{x}|}-\frac{1}{|\frac{1}{2}\mathbf{r}_1-\mathbf{x}|} \tag{5}$$

are the kinetic and potential energy operators in the center-of-mass frame. Here μ_{12} is defined as the reduced mass of particles 1 and 2, and $\mu_{12,3}$ as the reduced mass of particle 3 relative to particles 1 and 2:

$$\mu_{12}=\frac{m_1m_2}{m_1+m_2}\ ,\qquad \mu_{12,3}=\frac{(m_1+m_2)m_3}{m_1+m_2+m_3}\ . \tag{6}$$

In the latter equations, and hereafter, the two particles with equal charge (e^-e^-) are particles 1 and 2 while the opposite charged particle (positron) is particle number 3.

This choice of coordinates has two main advantages.

(1) The kinetic energy operator is simple, and can be separated in hyperspherical coordinates.

(2) When two of the three particles are identical, as is the case in Ps^-, $\mathbf{r}_1$ is chosen as the separation between the identical particles, so that the effect of the exchange operator is simple:

$$P_{12}f(\mathbf{r}_1,\mathbf{x})=f(-\mathbf{r}_1,\mathbf{x})\ . \tag{7}$$

The angular variables are chosen as the spherical angles $(\theta_1\phi_1)$ and $(\theta_2\phi_2)$ of the unit vectors $\hat{\mathbf{r}}_1$ and $\hat{\mathbf{x}}$.

III. HYPERSPHERICAL COORDINATES AND THE ADIABATIC TREATMENT

Hyperspherical coordinates (R,α) were first used in atomic physics to study the wave function of the helium atom in the limiting regime $\mathbf{r}_1\to\mathbf{0}$ and $\mathbf{r}_2\to\mathbf{0}$ (where $\mathbf{r}_1$ and $\mathbf{r}_2$ are independent-electron coordinates). They are defined by

$$R=(r_1^2+r_2^2)^{1/2}\ ,\qquad \alpha=\tan^{-1}(r_2/r_1)\ . \tag{8}$$

The only radial coordinate, R, represents the "size" of the system, while the mock angle α characterizes the radial correlation of the two electrons. Fock[10] showed later that the expansion of the ground-state wave function near $R=0$, the Fock expansion, contains terms which are powers of $\ln R$; this has been discussed more recently by Feagin and Macek.[11] Wannier[12] also used these coordinates in his study of electron-impact ionization of atoms near threshold. Starting with Macek's[13] adiabatic treatment of helium, hyperspherical coordinates have been used extensively and successfully for describing electron correlation and doubly excited states of atoms.[14,15]

When the three particles are of equal mass the hyperspherical coordinates R and α are defined as follows:[4,6,7]

$$R=(r_1^2+r_2^2)^{1/2}\ ,\qquad \alpha=\tan^{-1}(r_2/r_1)\ , \tag{9}$$

where

$$\mathbf{r}_2=c\mathbf{x}\ , \tag{10}$$

$\mathbf{r}_1$ and $\mathbf{x}$ are the Jacobi coordinates defined in the previous section, and the constant c is introduced so that the squared hyperspherical radius is proportional to the trace of the moment-of-inertia tensor of the system; this is a necessary condition for the kinetic energy to be separable in these coordinates[16,17]

$$c=(\mu_{12,3}/\mu_{12})^{1/2}=(\tfrac{4}{3})^{1/2}\ . \tag{11}$$

The kinetic and potential energy operators are then

$$T=-\frac{1}{2\mu_{12}}(\nabla_{r_1}^2+\nabla_{r_2}^2)=-\frac{1}{2\mu_{12}}\left[\frac{d^2}{dR^2}+\frac{5}{R}\frac{d}{dR}-\frac{\hat{\Lambda}^2}{R^2}\right], \tag{12}$$

$$V=\frac{1}{R\cos\alpha}-\frac{1}{R\left|\frac{1}{2}(\cos\alpha)\hat{\mathbf{r}}_1+\frac{1}{c}(\sin\alpha)\hat{\mathbf{r}}_2\right|}-\frac{1}{R\left|\frac{1}{2}(\cos\alpha)\hat{\mathbf{r}}_1-\frac{1}{c}(\sin\alpha)\hat{\mathbf{r}}_2\right|}\ ,$$

where $\hat{\Lambda}^2$ is the Casimir operator for the group O_6, usually called the "grand angular momentum operator:"

$$\hat{\Lambda}^2=-\frac{1}{\sin^2\alpha\cos^2\alpha}\frac{d}{d\alpha}\sin^2\alpha\cos^2\alpha\frac{d}{d\alpha}+\frac{l_1^2}{\cos^2\alpha}+\frac{l_2^2}{\sin^2\alpha}-\tfrac{1}{4}\ . \tag{13}$$

The Schrödinger equation is then

$$\left[\frac{1}{2\mu_{12}}\left[-\frac{\partial^2}{\partial R^2}-\frac{1}{R^2}\frac{\partial^2}{\partial\alpha^2}-\frac{1}{4R^2}+\frac{l_1^2}{R^2\cos^2\alpha}+\frac{l_2^2}{R^2\sin^2\alpha}\right]+V(R,\Omega)-E\right]\psi(R,\Omega)=0\ . \tag{14}$$

Here the usual wave function $\Psi(R,\Omega)$ has been renormalized[14] by setting

$$\psi(R,\Omega)=\Psi(R,\Omega)R^{5/2}\sin\alpha\cos\alpha \tag{15}$$

in order to remove first derivative terms in the kinetic energy operator both in R and in α. Ω stands for the angular variables

$$\Omega \equiv (\alpha, \hat{\mathbf{r}}_1, \hat{\mathbf{r}}_2) \ . \tag{16}$$

The R dependence of the potential energy in these coordinates factors out, so that $C(\Omega)$ is independent of R,

$$C(\Omega) = RV(R,\Omega) \ .$$

This fact will prove to be very important as the calculation of the matrix $\underline{C}$ can be done once and then used at all R values to calculate V, if an R-independent basis set is used.

Adiabatic expansion. In the hyperspherical approach,[13] the adiabatic treatment consists of solving the Schrödinger equation at *fixed hyperspherical radius* R in order to obtain the so-called adiabatic wave functions $\Phi_\mu(R,\Omega)$ and the adiabatic potential curves $U_\mu(R)$ as follows:

$$\hat{U}\Phi_\mu(R,\Omega) = U_\mu(R)\Phi_\mu(R,\Omega) \ , \tag{17}$$

where the fixed-R Hamiltonian $\hat{U}$ is

$$\hat{U} = \frac{\hat{\Lambda}'^2(\Omega)}{2\mu_{12}R^2} + \frac{C(\Omega)}{R} \tag{18}$$

and where $\hat{\Lambda}'^2$ is the grand angular momentum operator with the first derivative terms removed by rescaling the wave function in Eq. (15). The wave function is then expanded as

$$\psi(R,\Omega) = \sum_\mu F_\mu(R)\Phi_\mu(R,\Omega) \ . \tag{19}$$

When this expansion is entered into the Schrödinger equation, and is projected onto each of the $\Phi_\nu(R,\Omega)$, one gets a system of equations for the radial functions $F_\mu(R)$:

$$\frac{1}{2\mu_{12}}\left[-\frac{\partial^2}{\partial R^2}F_\nu(R) - \sum_\mu \left\langle \Phi_\nu \left| \frac{2\partial F_\mu}{\partial R}\frac{\partial}{\partial R} + F_\mu \frac{\partial^2}{\partial R^2} \right| \Phi_\mu \right\rangle \right] + [U_\nu(R) - E]F_\nu(R) = 0 \ . \tag{20}$$

where $\langle \ | \ \rangle$ implies integration over all angular variables. This is a system of n equations ($n \to \infty$ if the complete set is retained) coupled through the terms

$$W_{\mu\nu} = -\left\langle \Phi_\mu \left| \frac{\partial^2}{\partial R^2}\Phi_\nu \right\rangle \right. = -\frac{dP_{\mu\nu}}{dR} - (\underline{P}^2)_{\mu\nu} \tag{21}$$

and

$$P_{\mu\nu} = \left\langle \Phi_\mu \left| \frac{\partial}{\partial R}\Phi_\nu \right\rangle \right. \ . \tag{22}$$

Previous studies[14,18] have shown that the off-diagonal elements of the coupling matrix $P_{\mu\nu}$ ($P_{\mu\mu}=0$) are small everywhere in R except in the regions where two adiabatic curves try to cross, the so-called avoided-crossing regions. In this region the coupling term $P_{\mu\nu}$ becomes a leading term in the radial equation. Consequently, I have neglected the coupling between different channels everywhere except in the avoided-crossing regions. In these regions I have either forced the curves to cross diabatically when it is known (based on symmetry considerations) that the curves should cross, or else I have neglected the effects produced by this "avoided-crossing" and interpolate the curves adiabatically when it is known that the curves should not cross. The validity of this procedure will also be confirmed by the probability density plots.

The radial equation in this approximation is then

$$\left[\frac{1}{2\mu_{12}}\left[-\frac{\partial^2}{\partial R^2} + W_{\mu\mu}(R)\right] + U_\mu(R) - E\right]F_\mu(R) = 0 \ . \tag{23}$$

This equation can be integrated in order to obtain either resonance energy positions or scattering phase shifts, depending on the energy range of interest. Here the Numerov method has been used.

IV. SOLUTION OF THE ADIABATIC EIGENVALUE EQUATION

One of the most important intermediate results of the adiabatic hyperspherical treatment is the set of potential curves. They are analogous to the Born-Oppenheimer potential curves obtained in the study of diatomic molecules, except that the internuclear separation is replaced by the hyperspherical radius. These potential curves have permitted previous studies of three-particle systems to gain a deeper understanding of the dynamics.[14]

Different approaches have been presented in the literature for the solution of the adiabatic eigenvalue equation [Eq. (17)]. A method introduced by Macek[13] in his study of doubly excited states of helium ($\mu_{12}=1$), and used later in several studies,[16,19] consists of expanding the adiabatic wave functions $\Phi_\mu(R,\Omega)$ as

$$\Phi_\mu(R,\Omega) = \sum_{l_1,l_2} g^\mu_{l_1 l_2}(R,\alpha) Y_{l_1 l_2 LM}(\hat{\mathbf{r}}_1,\hat{\mathbf{r}}_2) \ , \tag{24}$$

where the $Y_{l_1 l_2 LM}(\hat{\mathbf{r}}_1,\hat{\mathbf{r}}_2)$ are standard coupled spherical harmonics. Substituting this equation into the adiabatic eigenvalue equation leads to a system of differential equations for $g^\mu_{l_1 l_2}(R,\alpha)$

$$\left[\frac{1}{2\mu_{12}R^2}\left[\frac{d^2}{d\alpha^2} - \frac{1}{4} + \frac{l_1(l_1+1)}{\cos^2\alpha} + \frac{l_2(l_2+1)}{\sin^2\alpha}\right] - U_\mu(R)\right] g^\mu_{l_1 l_2}(R,\alpha) = \sum_{l_1',l_2'} V_{l_1 l_2, l_1' l_2'} g^\mu_{l_1' l_2'}(R,\alpha) \ , \tag{25}$$

where

$$V_{l_1 l_2, l_1' l_2'} = \langle Y_{l_1 l_2 LM}(\hat{\mathbf{r}}_1,\hat{\mathbf{r}}_2) \mid V \mid Y_{l_1' l_2' LM}(\hat{\mathbf{r}}_1,\hat{\mathbf{r}}_2) \rangle \tag{26}$$

is an integral only over $\hat{\mathbf{r}}_1$ and $\hat{\mathbf{r}}_2$. When many partial waves have to be included, this method becomes inefficient, for one has to solve a large system of coupled dif-

ferential equations. A different approach, used first by Lin,[20] consists of expanding the adiabatic function in a basis of eigenfunctions of the grand angular momentum operator $\hat{\Lambda}^{\prime 2}$. These are, in this coordinate system, hyperspherical harmonics,[7,14] which form a complete set in $(\alpha,\hat{\mathbf{r}}_1,\hat{\mathbf{r}}_2)$:

$$y_{ml_1l_2}(\Omega)=N_{ml_1l_2}(\cos\alpha)^{l_1+1}(\sin\alpha)^{l_2+1}$$
$$\times F(-m,m+l_1+l_2+2,l_2+\tfrac{3}{2};\sin^2\alpha)$$
$$\times Y_{l_1l_2LM}(\hat{\mathbf{r}}_1,\hat{\mathbf{r}}_2)\chi_{SM_S}\ , \tag{27}$$

and correspond to eigenvalues of $\hat{\Lambda}^{\prime 2}$

$$(\lambda+2)^2-\tfrac{1}{4}=(2m+l_1+l_2+2)^2-\tfrac{1}{4}\ ,$$

where $m=0,1,2,\ldots$ is the number of nodes of (27) in α.

In Eq. (27) $N_{ml_1l_2}$ is a normalization constant, F is a hypergeometric polynomial, Y is a standard coupled spherical harmonic, and χ is a two-electron spinor. Some properties of these functions in this coordinate system are as follows: under interchange of particles 1 and 2,

$$\hat{P}_{12}y_{ml_1l_2}(\alpha,\hat{\mathbf{r}}_1,\hat{\mathbf{r}}_2)=y_{ml_1l_2}(\alpha,-\hat{\mathbf{r}}_1,\hat{\mathbf{r}}_2)$$
$$=(-1)^{l_1}y_{ml_1l_2}(\alpha,\hat{\mathbf{r}}_1,\hat{\mathbf{r}}_2)\ , \tag{28}$$

and under the parity operator,

$$\hat{\pi}y_{ml_1l_2}(\alpha,\hat{\mathbf{r}}_1,\hat{\mathbf{r}}_2)=(-1)^{l_1+l_2}y_{ml_1l_2}(\alpha,\hat{\mathbf{r}}_1,\hat{\mathbf{r}}_2)\ , \tag{29}$$

so that antisymmetry of the wave function under electron exchange is enfored by

$$(-1)^{S+l_1+1}=1\ .$$

The method introduced by Lin[20] diagonalizes $\hat{U}$ in a basis set consisting of these eigenfunctions of $\hat{\Lambda}^{\prime 2}$. This basis set has two advantageous properties: (i) $\hat{U}$ is almost diagonal in the limit $R\to 0$, where C/R is negligible compared to $[(\lambda+2)^2-\frac{1}{4}]/R^2$; and (ii) the basis functions $y_{ml_1l_2}(\Omega)$, like $C(\Omega)$, are independent of R, so that $\underline{C}$ must be calculated only once and can then be used to calculate matrix elements of $\hat{U}$ at all R values. Since the calculation of $\underline{C}$ is the most difficult and time-consuming part of the calculation, this is a very important property. This set also has a well-known disadvantage: its convergence at large R is extremely slow. The reasons for this slow convergence is the fact that the adiabatic wave function Φ_μ becomes confined into a very small portion of the (α,θ_{12}) plane, where it describes an atomic bound-state wave function. This is illustrated in Fig. 12 where I plot the probability density corresponding to Ps^- in the $^1P^o$ + state at $R=42$ a.u. Similar plots are obtained for different symmetries. The wave function is confined in the region $\alpha\simeq\pi/6$, $\theta_{12}\simeq 0,\pi$. These regions correspond to either electron being close to the positron and far from the other electron $[(e^--e^+)-e^-]$. This slow convergence implies that a large number of harmonics are needed; actually, as $R\to\infty$ an infinite number of harmonics would be required to reach convergence. In order to speed up this slow convergence, BG introduced a method which selects linear combinations of hyperspherical harmonics that are relevant to the physical configuration. This is accomplished by a "prediagonalization" of the matrix of the potential $\underline{C}$ in fixed-λ subspaces.

Prediagonalization. In this section I describe in detail a method introduced by BG for the variational solution of the adiabatic eigenvalue equation using a truncated basis of hyperspherical harmonics. As mentioned above, the main problem of this basis set is its extremely slow convergence, which means that large values of λ must be included. The problem is compounded by the fact that the dimensionality of the space increases rapidly as λ increases. For odd parity (with $L=1$), each successive eigenvalue contains one additional degenerate state $(m,l_1,l_2\equiv\eta)$, the actual degeneracy being $(\lambda+1)/2$ [see Fig. 2(a)]; for even parity (with $L=1$), every two succes-

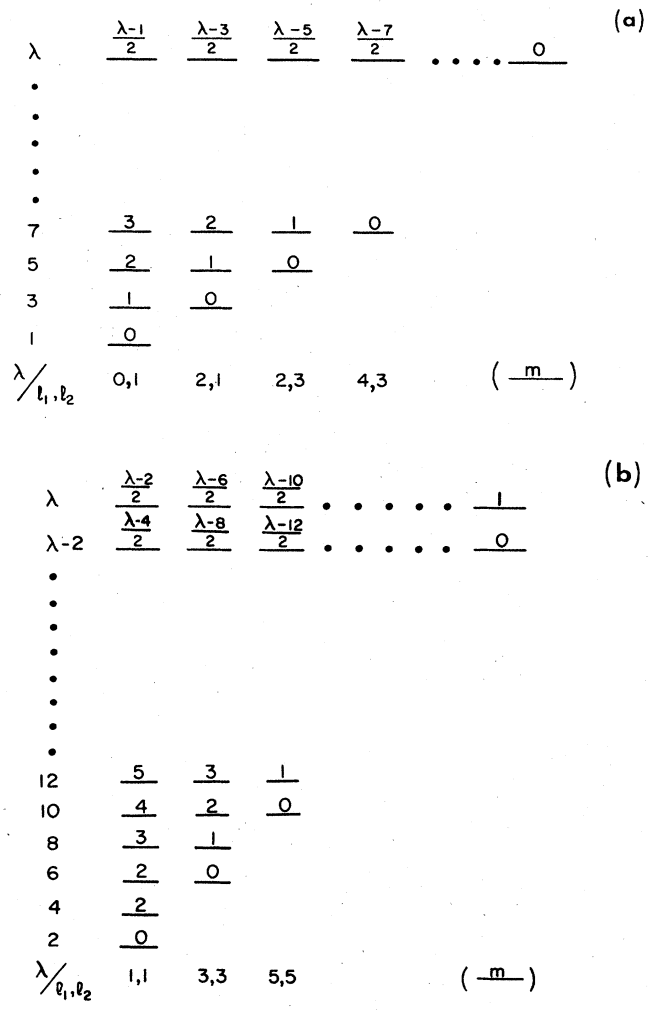

FIG. 2. (a) Degeneracy of the eigenvalues of $\hat{\Lambda}^{\prime 2}$ for an odd-parity singlet state with $L=1$. Each successive eigenvalue contains one additional degenerate state. (b) Degeneracy of the eigenvalues of $\hat{\Lambda}^{\prime 2}$ for an even-parity triplet state with $L=1$. Every two successive eigenvalues contain one additional degenerate state.

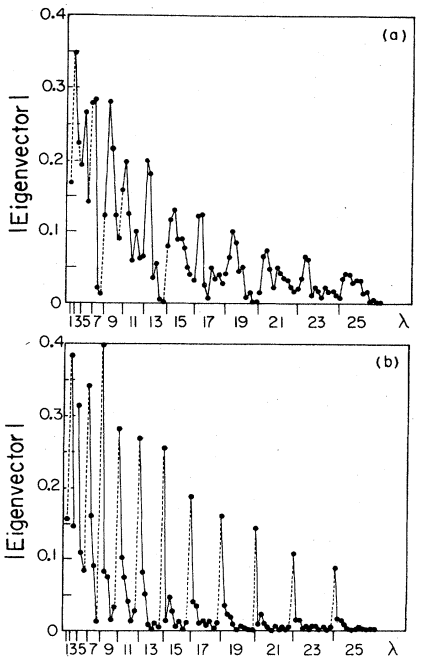

FIG. 3. Absolute values of the expansion coefficients of the lowest $^1P^o$ adiabatic eigenstate of Ps^- at $R=20$. Each dot corresponds to the coefficient of a single hyperspherical harmonic. In (a), the representation of harmonics used is that of Eq. (27). In (b) the prediagonalized representation is adopted instead (see text). (From Ref. 25.)

sive eigenvalues contain one additional degenerate state [see Fig. 2(b)]. Therefore, the dimensionality of the space increases in direct proportion to $\lambda_{\max}^2$. A way to circumvent this problem emerged in BG upon consideration of Fig. 3, which shows the absolute value of the eigenvector of $\hat{U}$ corresponding to the lowest eigenvalue U_1 at $R=20$ a.u. for the $^1P^o$ Ps^- system (analogous plots are obtained for each of the different systems studied here). Figure 3(a) shows the eigenvector $|z_{\eta,\mu}|$ in the "primitive" basis of hyperspherical harmonics. Notice how the components are distributed among most of the η's. Figure 3(b) shows eigenvector components $|z_{\lambda\nu,\mu}|$ of this same adiabatic eigenstate ($\mu=1$), but transformed into a different representation in which submatrices of the potential matrix $\underline{C}$ within a fixed-λ subspace are made diagonal. It is clear that only the eigenstates corresponding to the two or three lowest eigenvalues of each submatrix contribute appreciably to the adiabatic wave function. The reason why this prediagonalization sorts out the linear combination of physically relevant harmonics can be understood by considering the probability density plots corresponding to these states. The method used in calculating the density is presented in Appendix B. Figure 4 shows primitive basis functions corresponding to $\lambda=9$ and $l_1=4$, $l_2=5$, $m=0$ in (a) and $l_1=2$, $l_2=3$ and $m=2$ in (b), and $l_1=0$, $l_2=1$ and $m=4$ in (c). Notice how the density is distributed over the whole (α,θ_{12}) plane without any pattern relevant to physical considerations. Figure 5 shows prediagonalized basis functions in the $\lambda=19$ subspace. Figure 5(a) shows the density corresponding to the lowest eigenvalue. Notice how most of the density is distributed over the portions of the (α,θ_{12}) plane corresponding to physical configurations like $(e^- - e^+) - e^-$ ($\alpha \simeq \pi/6$, $\theta_{12} \simeq 0,\pi$). Figure 5(b) shows the density corresponding to the second lowest eigenvalue. Figure 5(f) shows the one corresponding to the highest eigenvalue. In this last case most of the density is in the region $\alpha \approx \pi/2$, which corresponds to the unphysical configuration $(e^- - e^-) - e^+$.

I have therefore truncated the basis set accordingly, retaining only the lower eigenstates in each λ subspace. Computational aspects of the method are detailed in Appendix A.

Next consider the nodal structure in θ_{12} that appears to be present in these prediagonalized eigenstates, even though this is a nonseparable problem, which means that the nodal structure in θ_{12} should not be independent of α

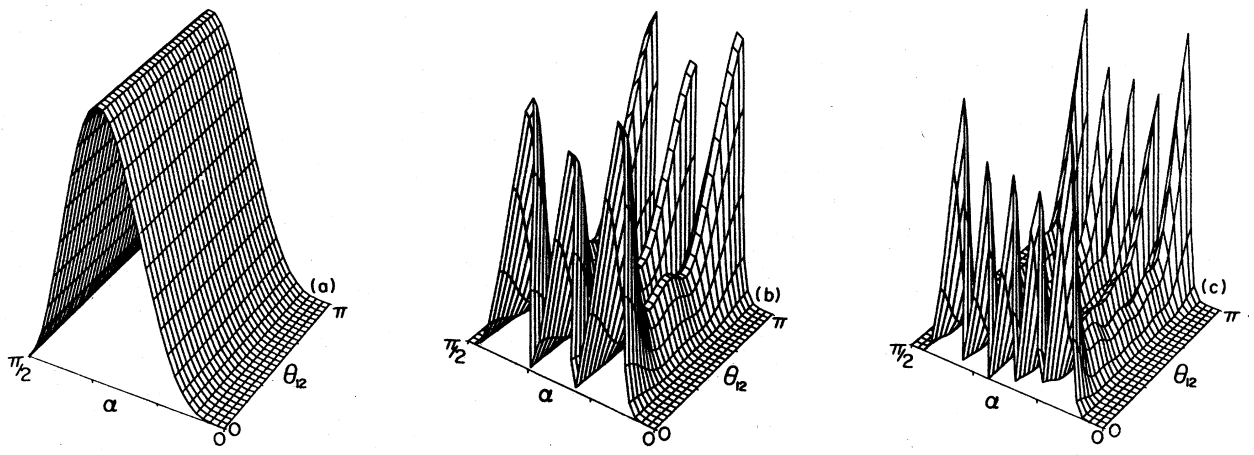

FIG. 4. Primitive squared basis functions (hyperspherical harmonics) in the $^1P^o$ $\lambda=9$ subspace. In (a) $l_1=4$, $l_2=5$, and $m=0$; in (b) $l_1=2$, $l_2=3$, and $m=2$; in (c) $l_1=0$, $l_2=1$, and $m=4$.

in general. Nevertheless, such a pattern seems to exist. Figure 5 shows plots of the density corresponding to states in the $\lambda=19$ subspace. The states correspond to the lowest, second, fourth, sixth, eighth and highest eigenvalues in (a), (b), (c), (d), (e), and (f), respectively. The state corresponding to the highest eigenvalue has no nodes in θ_{12}, and the number of nodes increases as the eigenvalue decreases down to a point where that "symmetry" is broken. This pattern is the same in all λ subspaces. An analogous pattern is observed when one plots all the eigenvalues in an energy-versus-λ plot.[21] Figure 6 shows this plot for the $^1P^o$ Ps^- system up to $\lambda=35$. Each line corresponds to the position of one eigenvalue in the corresponding λ subspace. The upper half of the "spectrum" follows some regularity while the lower part apparently does not. Notice that the eigenstates in which the nodal structure is lost is apparently the same state where the regularity in the E-λ plot is lost (for example, when $\lambda=19$, this occurs in the third lowest eigenstate). The reason why this regularity in the nodal structure exists is still not understood but suggests that the problem may be quasiseparable, at least for those states that have large amplitude in the high prediagonalized eigenstates. This kind of regular and chaotic behavior of the spectrum of the Hamiltonian has been studied by Stefanski and Taylor[22] for a classical Hamiltonian. A similar "prediagonalization" was introduced, parallel to BG, in the problem of a hydrogen atom in a magnetic field.[23] There, the prediagonalization was made in subspaces with n fixed, where n is the principal quantum number of the hydrogen atom.

Large-R limit of the potential curves. In the limit $R\rightarrow\infty$ (and $E<0$) the physical configuration of the system is an electron far from a neutral atom. In the Jacobi coordinates described above, this limit implies that both r_1 and r_2 go to infinity. This suggests the use, in this limiting region, of a different set of coordinates in which the physical configuration is represented more clearly. In this new set of coordinates $\mathbf{r}_1'$ is the position vector of electron 1 with respect to the nucleus (e^+) and $\mathbf{x}'$ is the position vector of electron 2 with respect to the center of mass of the atom. Notice that this new set is identical to the independent-particle coordinate system mentioned before, when the nucleus is infinitely massive.

A new set of hyperspherical coordinates analogous to R and α is defined as follows:

$$R'^2=r_1'^2+r_2'^2\ ,$$
$$\alpha'=\tan^{-1}(r_2'/r_1')\ , \tag{30}$$

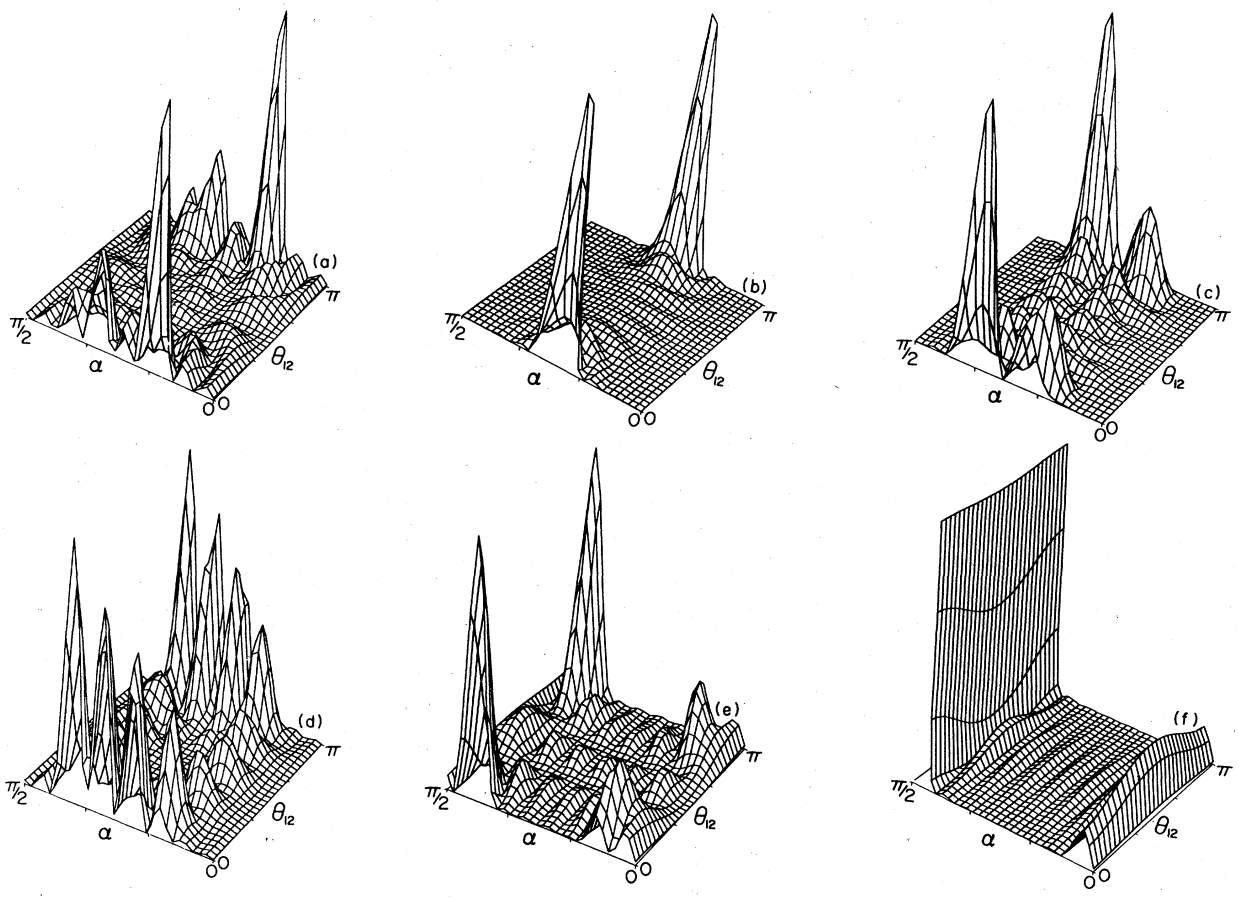

FIG. 5. Probability density corresponding to $^1P^o$ prediagonalized basis functions. In (a) is the density corresponding to the lowest eigenvalue. In (f) is the one corresponding to the highest eigenvalue (see text).

where

$$\mathbf{r}'_2 = c'\mathbf{x}' ,$$

$$c' = (\mu_{13,2}/\mu_{13})^{1/2} = (\tfrac{4}{3})^{1/2} . \tag{31}$$

Since the squared hyperspherical radius is defined such that it is proportional to the trace of the moment-of-inertia tensor of the systems, R'^2 must be proportional to R^2, i.e., $R'^2 = dR^2$. The constant of proportionality was found to be

$$d = \frac{1}{c^2} + \tfrac{1}{4} = 1 \tag{32}$$

by expressing R'^2 in terms of r_1^2 and r_2^2. The hyperspherical radius R enters the adiabatic equation only as a parameter. Therefore the only effect of this transformation of coordinates is a scaling of the abscissas of the potential curves by a factor $d^{1/2}$.

The asymptotic limit of these new coordinates is

$$\langle r'_1 \rangle \to \text{const} ,$$

$$r'_2 \to R' , \tag{33}$$

$$\alpha' \to \pi/2, \quad \alpha'' = \alpha' - \pi/2 \to 0$$

as $R \to \infty$, provided the total energy is negative.

In order to see the asymptotic limit of the adiabatic equation, I set $\rho = R'\alpha''$ and expand in powers of $1/R'$, obtaining[13]

$$\left\{ \left[\frac{1}{2\mu_{13}} \left[-\frac{\partial^2}{\partial\rho^2} + \frac{l'^2_1}{\rho^2} \right] - \frac{1}{\rho} \right] + \frac{1}{R'^2} \left[\frac{1}{2\mu_{13}} \left[-\tfrac{1}{4} + \frac{l'^2_1}{3} + l'^2_2 \right] + c'^2 \rho \hat{\mathbf{r}}'_1 \cdot \hat{\mathbf{r}}'_2 - \frac{\rho}{6} \right] + O(1/R'^3) \right\} \Phi_\mu(R', \Omega')$$

$$= U_\mu(R') \Phi_\mu(R', \Omega') . \tag{34}$$

The terms inside the first square brackets coincide with the atomic Hamiltonian when I set $r'_1 \simeq \rho$. It has been proved in the appendix of Ref. 13 that, to order $1/R^2$, the potential in the large-R limit is the same as that obtained from the close-coupling equations for states of the same principal quantum number. This means that, when including the adiabatic correction in Eq. (34), the term proportional to $1/R'^2$ is

$$\hat{D} = \frac{1}{2\mu_{13}} l'^2_2 + c'^2 \mathbf{r}'_1 \cdot \hat{\mathbf{r}}'_2 , \tag{35}$$

where I have also set $r'_1 \simeq \rho$. The effect of this term on the adiabatic potential curve can be calculated using degenerate perturbation theory. This amounts to finding the eigenvalues of the operator $\hat{D}$ in the corresponding $n-L$ subspace. Here n is the principal quantum number of the atom and L is the total angular momentum of the system. This is the standard procedure of Seaton[24] and of Gailitis and Damburg.[25]

V. RESULTS AND DISCUSSION

A. $^1S^e$ symmetry

The ground state of Ps^- has a $^1S^e$ symmetry. This requires l_1 and l_2 to be even and equal, so that λ is also

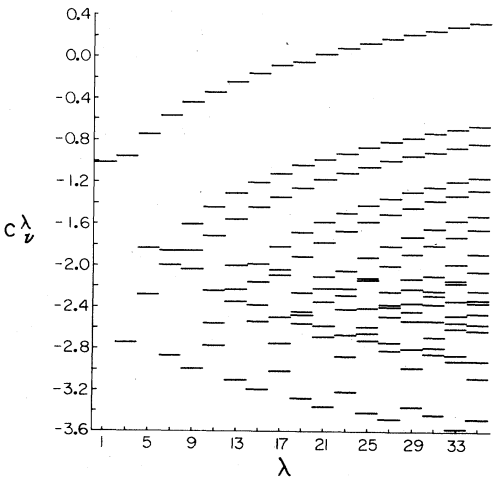

FIG. 6. Each line corresponds to the position of one eigenvalue of c^λ in the corresponding λ subspace (see text).

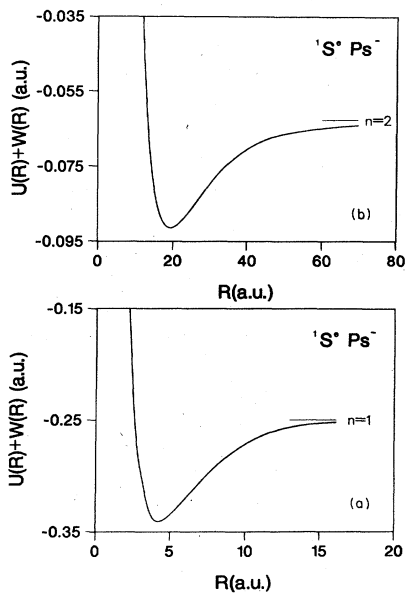

FIG. 7. The lowest two $^1S^e$ hyperspherical potential curves of Ps^- converging to the (a) $n=1$ and (b) $n=2$ threshold of Ps.

even (including $\lambda=0$). The ground-state potential curve, $U_1(R)+W_{11}(R)$, is shown in Fig. 7(a). It has been proved (see Appendix of Ref. 26) that the solution of the radial equation [Eq. (23)] gives a lower bound on the lowest exact energy for each symmetry (assuming that the potential curves are perfectly converged) when the adiabatic correction term $W_{11}(R)$ is not included, and gives an upper bound when the adiabatic correction term is included. At large R, $R \geq 15$, the curve was smoothly connected to the one calculated using the method presented in Ref. 6, in which an asymptotic basis is used. The asymptotic basis helps to obtain a better-converged curve in this region with a much smaller number of basis functions. At small R, $R<15$ a.u., the two curves are almost exactly the same. The lower and upper bounds on the ground-state energy obtained were $E_l=-0.2646$ and $E_u=-0.2597$ a.u., which bracket the best calculated value $E=-0.2620$ a.u. (Ref. 27).

The lowest $^1S^e$ potential curve converging to the $n=2$ threshold of Ps is shown in Fig. 7(b). It has a minimum at $R=20$ a.u. and behaves asymptotically as $-7.06/R^2$ below threshold. It supports an infinite number of Feshbach resonances, owing to the long-range dipole attraction, the lowest of which was calculated to be $E=-0.0763$ a.u., in good agreement with a previous calculation using the complex-coordinate rotation method[28] $E=-0.076\,02$ a.u. There is a second curve converging to the same threshold which is completely repulsive and behaves asymptotically as $10.06/R^2$ above threshold.

B. $^1P^o$ symmetry

Photodetachment of the ground state of Ps^- leads to $^1P^o$ symmetry in the final state, since the transition

$$h\nu+\mathrm{Ps}^-(1s^2\,{}^1S^e)\rightarrow \mathrm{Ps}^-(^1P^o)\rightarrow e+\mathrm{Ps}$$

is the only allowed dipole transition. By analyzing the potential curves obtained with the method described in earlier sections, BG was able to predict the main resonance features which should be seen in Ps^- photodetachment. The results obtained there will be discussed here along with probability density plots, which corroborate the diabatic interpolation of the + and − potential curves.

This symmetry requires l_1 to be even and l_2 to be odd, so that λ is odd as well. The potential curves $U_\mu(R)+W_{\mu\mu}(R)$ are shown in Fig. 8. (The ground state, a completely repulsive curve converging to the ground state of Ps, is not shown.) As explained in Sec. IV, these potential curves were connected smoothly to their asymptotic form at $R>45$ a.u. These potential curves and those for H^- calculated by Lin[29] and by Klar and Klar[30] and also by the author[4] using the method presented here are qualitatively similar, apart from numerical values, so the same classification (+, −, and pd) introduced by Cooper, Fano, and Prats[31] is used here.

The von Neuman–Wigner noncrossing rule states that adiabatic potential curves belonging to the same symmetry cannot cross.[32] The + and − curves do not strictly have different symmetry, so they cannot cross. In fact, they show an avoided crossing at $R=35.5$ a.u. with a minimum separation of $\Delta U=0.0012$ a.u. The diabatic interpolation in the region $28<R<42$ made in Fig. 8 is based on the fact that the system does not behave adiabatically in regions of avoided crossings[18] where two adiabatic channels interact strongly. In order to corroborate this, I present plots of the probability density corresponding to the + and − states before and after the crossing. Figure 9 shows the density plot corresponding to the + state at $R=20$ a.u. (before the crossing), and Fig. 10 shows the one corresponding to the − state at $R=25$ a.u. (also, before the crossing). Notice the big difference between these two plots. The − character is mainly expressed by the presence of an approximate node at $\theta_{12}=\pi/2$ (this corresponds to a node at $\alpha=\pi/4$ in Macek's coordinates or to $r_1=r_2$ in independent-particle coordinates), and the + character by the absence of this node (at small R, there is an antinode at $\theta_{12}=\pi/2$). Figure 11 shows the − potential curve (e.g., the potential curve corresponding to the second lowest eigenvalue, rather than the third) at $R=42$ a.u. Notice that the node at $\theta_{12}=\pi/2$ is still present. Figure 12 shows the + potential curve at the same R value. Notice the absence of a node at $\theta_{12}=\pi/2$. This strongly suggests that the diabatic interpolation is correct. The position and width of the shape resonance supported by the + potential curve and the two lowest Feshbach resonances supported by the − potential curve were reported in BG.

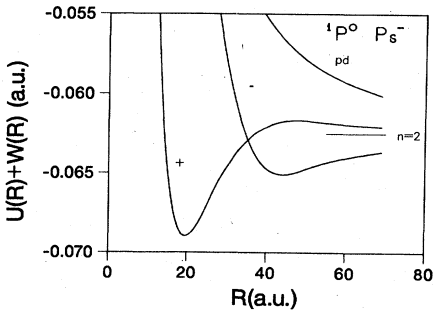

FIG. 8. The $^1P^o$ hyperspherical potential curves of Ps^- converging to the Ps ($n=2$) threshold. (From Ref. 25.)

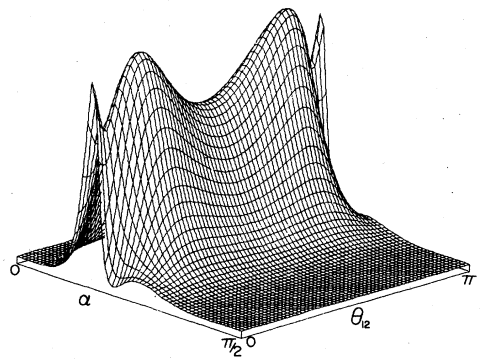

FIG. 9. Probability density of the $^1P^o$ + channel of Ps^- at $R=20$ a.u. (before the crossing between the + and − potential curves).

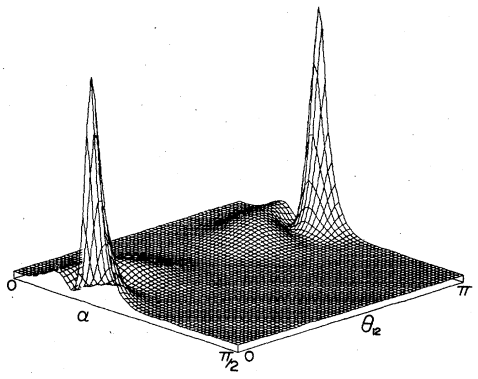

FIG. 10. Probability density of the $^1P^o$ − channel of Ps^- at $R=25$ a.u. (before the crossing between the + and − potential curves).

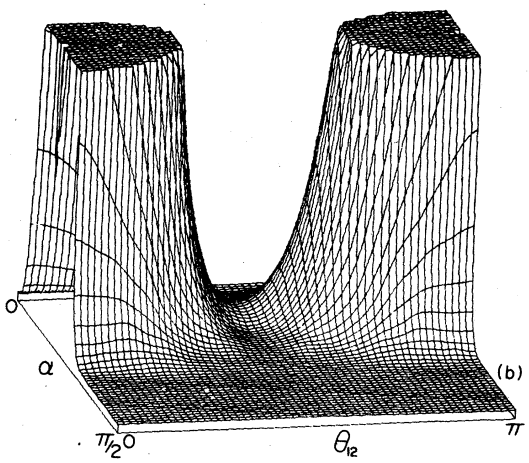

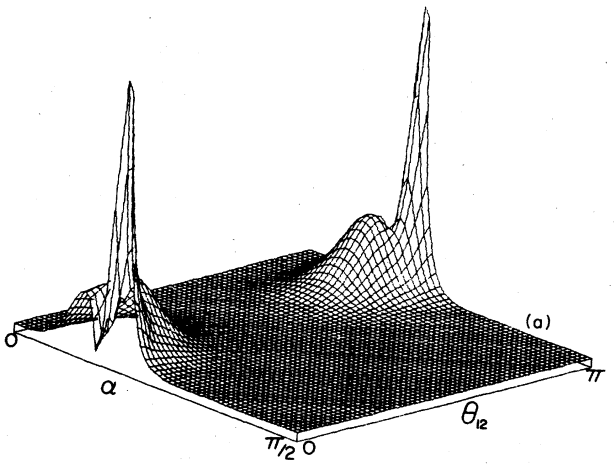

FIG. 11. Probability density of the $^1P^o$ − channel of Ps^- at $R=42$ a.u. (after the crossing between the + and − potential curves). In (b), the plot has been cut at $\rho=0.025$ in order to see more clearly the approximate node at $\theta_{12}=\pi/2$.

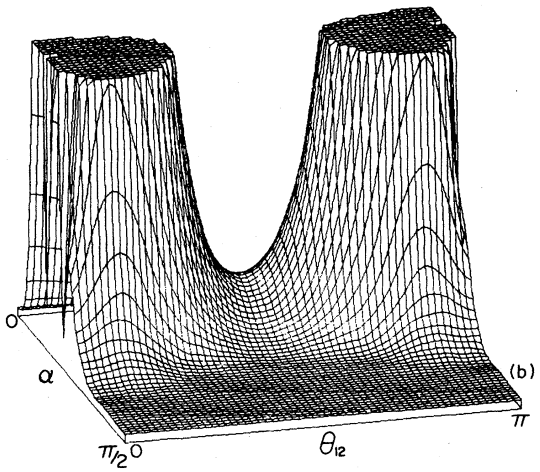

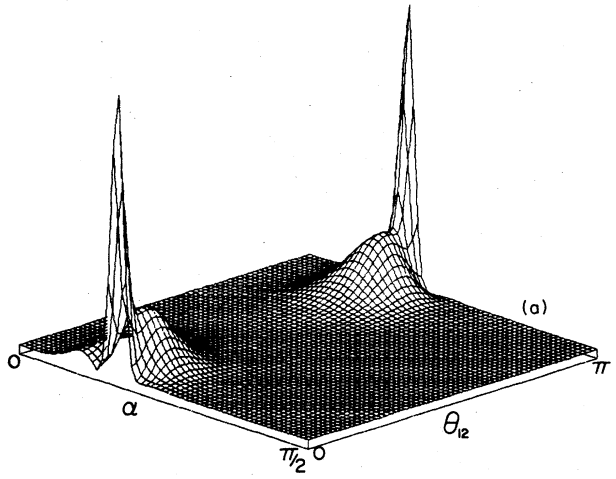

FIG. 12. Probability density of the $^1P^o$ + channel of Ps^- at $R=42$ a.u. (after the crossing between the + and − potential curves). In (b), the plot has been cut at $\rho=0.025$ in order to see the absence of a node at $\theta_{12}=\pi/2$.

C. $^3P^e$ symmetry

The existence of a metastable $2p^2\,^3P^e$ state of Ps^- would have many experimental implications, for it would not decay by two-photon electron-positron annihilation (in first order) but rather by a slow radiative transition to an

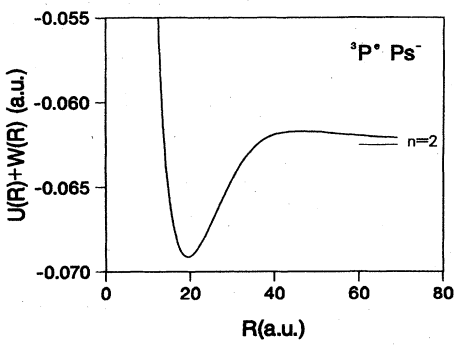

FIG. 13. The lowest hyperspherical potential curve for Ps^-, $^3P^e$ symmetry, converging to the Ps ($n=2$) threshold.

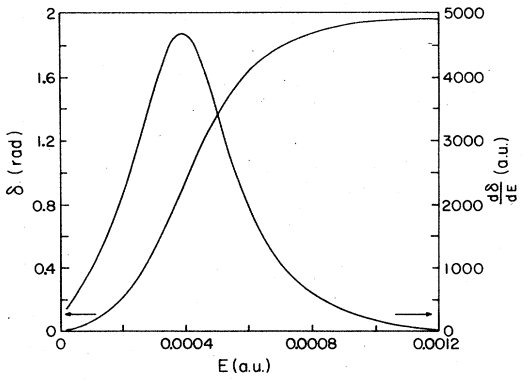

FIG. 14. The elastic scattering phase shift and its energy derivative just above the Ps ($n=2$) threshold for $^3P^e$ symmetry of Ps^-. These indicate a shape resonance at an energy of 3.7×10^{-4} a.u. above threshold.

autoionizing state.[33] Two previous studies[27,33] have not found such a state. In this calculation I confirm these studies, and find the reason for the absence of such a state: it has become a shape resonance. In this case, l_1 is odd, l_2 is odd, and λ is even and nonzero.

Figure 13 shows the lowest potential curve corresponding to $^3P^e$ symmetry converging to the $n=2$ threshold of Ps. Much like the $^1P^o$ + channel,[7] the $^3P^e$ potential curve is not sufficiently deep to support a metastable state, but it does support a shape resonance at an energy $E=3.8\times10^{-4}$ a.u. above threshold. Figure 14 shows the calculated elastic scattering phase shifts and the time delay, from which the width of the resonance (coming also from tunneling through the barrier) can be obtained, $\Gamma=3.6\times10^{-4}$ a.u. Figure 15 shows the probability density at $R=20$ a.u. (at about the minimum of the potential curve). The results of this calculation confirm the super-

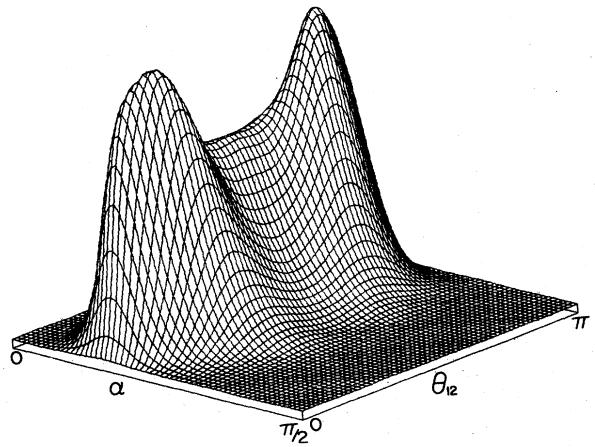

FIG. 15. Probability density of the lowest $^3P^e$ state of Ps^- at $R=20$ a.u.

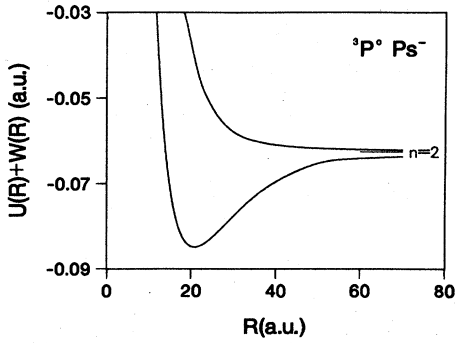

FIG. 16. Lowest two of the three $^3P^o$ hyperspherical potential curves of Ps^- which converge to the Ps ($n=2$) threshold.

multiplet classification of Herrick *et al.*[34] in which the $^3P^e$ and the $^1P^o$ are part of a supermultiplet in H^-, since the $^1P^o$ resonance lies very close in energy to the $^3P^e$ resonance. The same resemblance exists in the probability density as can be seen by comparing Figs. 15 and 9, even though a remarkable difference exists at $\theta_{12}=0$ and π, where the density corresponding to the $^3P^e$ state is constrained to vanish while the $^1P^o$ + state is nonzero there. These symmetry constraints can be understood by analogy with the exclusion of parity unfavored transitions in forward (or backward) scattering collisions, explained by Fano in 1964.[35] A second difference between the probability density plots corresponding to the $^1P^o$ + and the $^3P^e$ states is the presence of an extra node in the $^1P^o$ state. This can be understood with the help of the independent-electron picture, where the $^1P^o$ is a linear combination of $2s\varepsilon p+2p\varepsilon s$ with some $2p\varepsilon d$ and has a node in the $2s$ function, while the $^3P^e$ is basically $2p^2$ and has no nodes.

D. $^3P^o$ symmetry

In both He and H^-,[34] the $^3P^o$ symmetry holds a quasibound state which has the strongest binding of all of the P doubly excited states near the $n=2$ threshold. The same is expected for Ps^-. This symmetry requires l_1 to be odd and l_2 to be even so that λ is also odd.

The two lowest potential curves converging to the $n=2$ threshold of Ps are shown in Fig. 16. The + channel is much more attractive than in the $^1P^o$ + case; the minimum of the $^3P^o$ potential curve is $U_2+W_{22}=-0.085$ a.u. at $R=20$ a.u. compared to $U_2+W_{22}=-0.069$ at $R=20$ for $^1P^o$. This is consistent with Hund's rule, which states that all else being equal, triplet atomic states lie lower than singlets, since the Pauli principle keeps the electrons farther apart in the triplet state. The coupling between the + and − channels in the avoided crossing region, $R\approx45$, is much smaller for the $^3P^o$ than for $^1P^o$, and the system therefore behaves adiabatically. This can again be illustrated with the probability density. Figure 17 shows the density corresponding to the + channel at $R=20$ a.u., before the avoided crossing region, in (a), and at $R=50$ a.u., after the avoided crossing region, in (b). Figure 18 shows the density corresponding to the − channel at $R=25$ a.u. in (a) and

at $R=50$ a.u. in (b). Notice how the characteristic properties of each channel are conserved through the avoided-crossing region, strongly suggesting that the two potential curves do not cross (as in He and H^-). Therefore the potential curves were adiabatically interpolated in the region $38<R<50$. At large R, the potential curves were smoothly connected with the asymptotic curves, just as in the $^1P^o$ case.

The + potential curve, the only attractive one, is now deep enough to support quasibound states below the $n=2$ threshold of Ps. It supports an infinite number of resonances (nonrelativistically). The three lowest were found by numerically integrating the radial equation giving $E_1=1.03\times10^{-2}$ a.u., $E_2=4.5\times10^{-4}$ a.u., and $E_3=9\times10^{-5}$ a.u. below the $n=2$ threshold, the lowest two of which are in good agreement with another calculation.[36] The binding energy of successive resonances decreases exponentially to zero. The − potential curve is in this case completely repulsive, as is the pd curve (which is not shown in Fig. 16), and they do not hold any resonances.

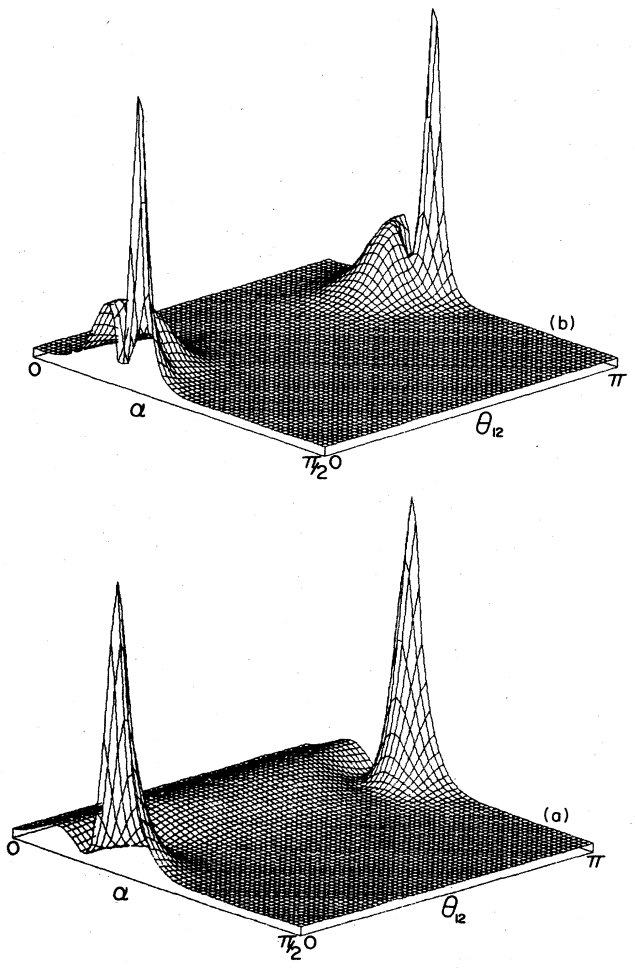

FIG. 17. Probability density of the $^3P^o$ + channel of Ps^-. In (a) $R=20$ a.u. while in (b) $R=50$ a.u. (see text).

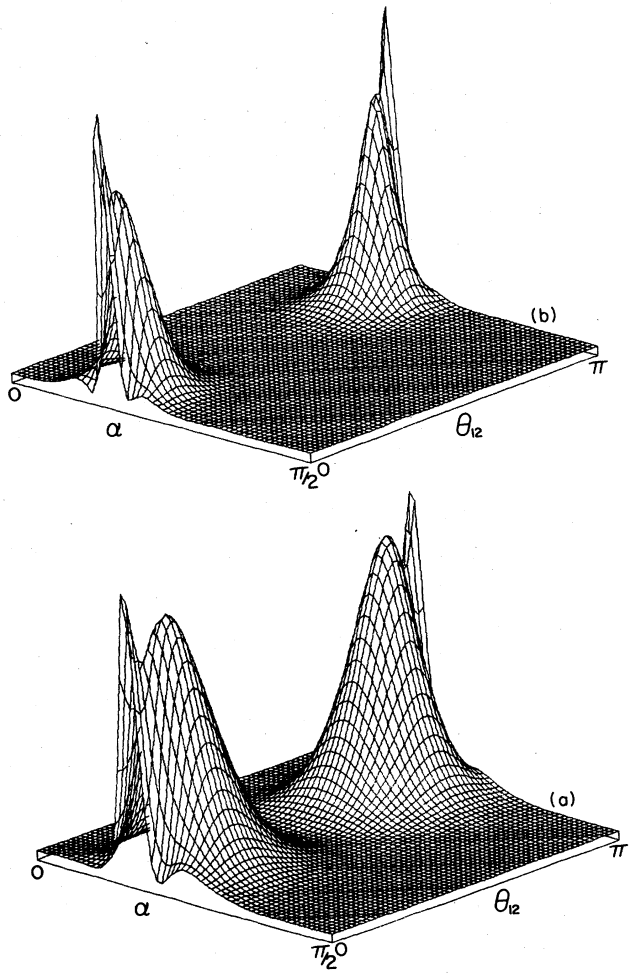

FIG. 18. Probability density of the $^3P^o$ − channel. In (a) $R=25$ a.u. while in (b) $R=50$ a.u. (see text).

E. $^1D^e$ symmetry

In H^- the symmetry holding the most deeply bound resonant state after $^3P^o$ is $^1D^e$. In view of all of the similarities seen thus far, the same is expected in Ps^-. Symmetry requires l_1 and l_2 to be even so that λ is also even and nonzero. The degeneracy in each λ subspace is even higher in this case, since the orbital angular momentum is $L=2$. Figure 19 shows how the degeneracy increases as λ increases. In this case, the use of the prediagonalized basis is even more necessary, since the number of "primitive" basis functions required to reach convergence was more than 800.

The potential curves converging to the $n=2$ threshold of Ps are shown in Fig. 20. (The ground-state curve, a completely repulsive curve converging to the $n=1$ threshold of Ps, is not shown.) These curves are like those corresponding to the $^3P^o$ symmetry, but not as deep. The lowest curve shown (the + curve) has a minimum $U_2+W_{22}=-0.078$ a.u. at $R=20$ a.u. In this case there is no avoided crossing at large R and the curves behave adiabatically. At small R there is an avoided crossing at

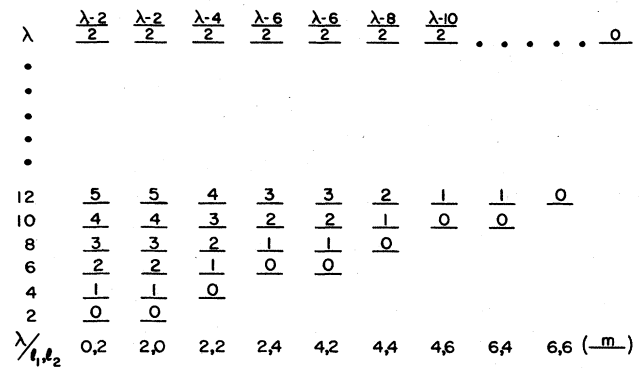

FIG. 19. Degeneracy of the eigenvalues of $\hat{\Lambda}^{'2}$ for an even-parity singlet state with $L=2$.

$R=10$ a.u. (It does not appear in Fig. 20 because it is at higher energy.) At large R, the curves were smoothly connected to their asymptotic limit. For this symmetry with $L=2$, the three channels in the $n=2$ subspace in the independent-electron picture are $2s\varepsilon d$, $2p\varepsilon p$, and $2p\varepsilon f$. As for $^3P^o$ symmetry, the only attractive curve is the one corresponding to $\mu=2$. It supports an infinite number of resonances as is guaranteed by the long-range dipole attraction which behaves at large R as $1.44/R^2$. The lowest of these was calculated to be $E_1=-0.067\,243$ a.u. by numerically integrating the radial equation. The other two curves are completely repulsive and behave asymptotically as $6/R^2$ and $9.44/R^2$, respectively.

VI. CONCLUSIONS

The present analysis has shown the existence of many resonance states in Ps^-. While most previous studies using hyperspherical coordinates were aimed at understanding features of electron correlations in doubly excited states which were obtained from more sophisticated calculations or from experiment, the present study relies only on the hyperspherical potential curves to predict these resonance features. From the $^3P^e$ potential curve, it can now be understood why previous studies[27,33] have not found a quasibound state below the $n=2$ threshold corresponding to the known $2p^2\,^3P^e$ metastable state of H^-. The potential curve is not attractive enough to support a level below threshold, but rather it supports a shape resonance above threshold instead. As for the $^1P^o$ shape resonance,[7] the $^3P^e$ shape resonance decay width comes primarily from tunneling through the barrier. The $^3P^e$ and $^1D^e$ potential curves show that there is no possible shape resonance in these symmetries (near the $n=2$ threshold), as there is none in H^-, since the + and − curves behave adiabatically, and therefore there is only one attractive curve (+), which supports an infinite number of Feshbach resonances. The spectrum of Ps^- presented here is very similar to the spectrum of H^-, in the sense that it follows the same order: $^1S^e$, $^3P^o$, $^1D^e$, $^1P^o$ −, $^3P^e$, $^1P^o$ +. Table I shows the binding energy of Ps^- and H^- resonances in the different symmetries studied here. As can be seen in the table, the scaling factor of approximately one-half does not hold for all symmetries. A study of other three-particle systems, including the recently observed muonium negative ion,[37] using the method presented in this paper[38] shows a remarkably *linear* dependence of the binding energy of three-particle systems on the atomic reduced mass.

The prediagonalization method, introduced by BG and used in this analysis, should prove very useful in the study of many-particle systems, since it exploits the degeneracy of the adiabatic eigenvalues in one region ($R\to 0$) of configuration space. It enables one to choose only those eigenstates in each degenerate subspace which have a high density in the region where the potential is minimum. Lastly, the method introduced in Appendix B for calculating the body-fixed probability density should also prove useful in the study of other three-particle systems, since it is not restricted in any way to the Jacobi coordinates used in this work.

ACKNOWLEDGMENTS

I want to express my deep gratitude to Dr. Chris H. Greene for suggesting this problem, for his continual guidance and support, and for his editorial help during the

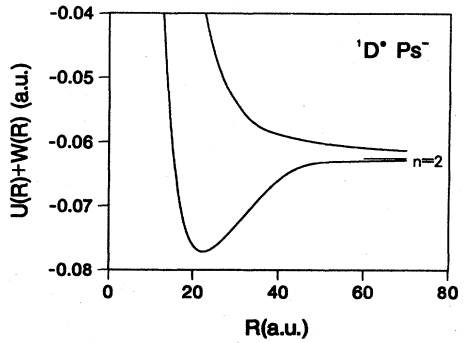

FIG. 20. Lowest two of the three $^1D^e$ hyperspherical potential curves of Ps^- which converge to the Ps ($n=2$) threshold.

TABLE I. Binding energy of Ps^- and H^- for different symmetries (in a.u.).

	Binding energy (a.u.)	
	Ps^-	H^-
$^1S^e$ ($\mu=1$)	0.0120[a]	0.027 56[b]
$^1S^e$ ($\mu=2$)	0.0139	0.0237[c]
$^3P^o$	0.0103	0.0171[c]
$^1D^e$	0.004 93	0.002 78[c]
$^1P^o$	0.000 087	0.001 04[d]

[a]Reference 27.
[b]Reference 42.
[c]Reference 43.
[d]Reference 44.

writing of this paper. I also acknowledge several useful conversations with Dr. A. R. P. Rau, Dr. Y. K. Ho, and Dr. M. Lawen, I acknowledge support from the Fulbright Commission and from the Escuela Colombiana de Ingenieria, from which I have been on a leave of absence. This work was partially supported by the National Science Foundation. The computational work was performed on a Ridge 32 system and on the IBM 3084 of the System Network Computer Center of Louisiana State University. Thanks to N. N. Choi for pointing out the misprint in Ref. 6.

APPENDIX A: COMPUTATION OF $U_{ml_1l_2,m'l_1'l_2'}$

As explained in the text, the diagonalization of $\hat{U}$ is made here in two steps. First, the potential matrix $\underline{C}$ is diagonalized within degenerate λ subspaces in the primitive basis, e.g., the hyperspherical harmonics of Eq. (27). This amounts to diagonalizing submatrices c^{λ} with dimensions given by the degeneracy of the corresponding λ subspace.

In order to calculate the matrix elements of c^{λ}, $\underline{C}$ was expanded as follows:

$$\underline{C}=RV=\frac{1}{\cos\alpha}-\frac{R}{\left|\frac{1}{2}\mathbf{r}_1+\frac{1}{c}\mathbf{r}_2\right|}-\frac{R}{\left|\frac{1}{2}\mathbf{r}_1-\frac{1}{c}\mathbf{r}_2\right|},$$

$$\underline{C}=\frac{1}{\cos\alpha}-2\sum_{k=0}^{\infty}{}'\frac{r_<^k}{r_>^{k+1}}P_k(\cos\theta_{12}), \tag{A1}$$

where $r_<$ ($r_>$) is the lesser (greater) of $\frac{1}{2}\cos\alpha$ and $(1/c)\sin\alpha$, and $\sum'$ implies summation over even values of k only. Then

$$c^{\lambda}_{\eta,\eta'}=\langle\eta\,|\,\underline{C}\,|\,\eta'\rangle^{\lambda}, \tag{A2}$$

$$c^{\lambda}_{\eta,\eta'}=N_{ml_1l_2}N_{m'l_1'l_2'}\int_0^{\pi/2}d\alpha\,F(-m,m+l_1+l_2+2,l_2+\tfrac{3}{2},\sin^2\alpha)F(-m',m'+l_1'+l_2'+2,l_2'+\tfrac{3}{2},\sin^2\alpha)$$
$$\times(\cos\alpha)^{l_1+l_1'+2}(\sin\alpha)^{l_2+l_2'+2}\left[\frac{1}{\cos\alpha}\delta_{l_1l_1'}\delta_{l_2l_2'}-2\sum_k{}'\frac{r_<^k}{r_>^{k+1}}\beta(l_1l_2l_1'l_2';kLM)\right] \tag{A3}$$

with

$$2m+l_1+l_2=\lambda \tag{A4}$$

and where I have defined an integral over $\hat{\mathbf{r}}_1$ and $\hat{\mathbf{r}}_2$ to be

$$\beta(l_1l_2l_1'l_2';kLM)=\langle Y_{l_1l_2LM}\,|\,P_k(\cos\theta_{12})\,|\,Y_{l_1'l_2'LM}\rangle \tag{A5}$$

which was evaluated using Eq. (13.63) of Sobel'man.[39]

The expansion of the hypergeometric polynomials used for the computation of $c^{\lambda}_{\eta,\eta'}$ is[20]

$$F(-m,m+l_1+l_2+2,l_2+\tfrac{3}{2};\sin^2\alpha)$$
$$=\frac{\Gamma(m+1)\Gamma(l_2+\frac{3}{2})}{\Gamma(m+l_2+\frac{3}{2})}\times\sum_{s=0}^{m}(-1)^{m-s}\begin{bmatrix}m+l_2+\frac{1}{2}\\ s\end{bmatrix}\begin{bmatrix}m+l_1+\frac{1}{2}\\ m-s\end{bmatrix}$$
$$\times(\cos\alpha)^{2s}(\sin\alpha)^{2(m-s)}. \tag{A6}$$

This expression becomes unstable at $\sin^2\alpha\cong 1$ when $m\gtrsim 20$. For this reason, I use the expression[40]

$$F(-m,m+l_1+l_2+2,l_2+\tfrac{3}{2};\sin^2\alpha)$$
$$=(-1)^m\frac{\Gamma(m+l_1-\frac{1}{2})\Gamma(l_2-\frac{1}{2})}{\Gamma(m+l_2-\frac{1}{2})\Gamma(l_1-\frac{1}{2})}$$
$$\times F(-m,m+l_1+l_2+2;l_1+\tfrac{3}{2};1-\sin^2\alpha) \tag{A7}$$

for all values of m where $\sin^2\alpha>0.5$. When $m\gtrsim 27$, this expression is unstable as well in the region $\sin^2\alpha\sim 0.5$. In this regime, I then used an asymptotic expression for the hypergeometric function[41] for values of α in the region $0.1<\sin^2\alpha<0.9$:

$$F(-m,m+l_1+l_2+2;l_2+\tfrac{3}{2};\sin^2\alpha)$$
$$=\frac{1}{\begin{bmatrix}m+l_2+\frac{1}{2}\\ m\end{bmatrix}}\times\frac{\cos[(2m+l_1+l_2+2)\alpha-(l_2+\frac{1}{2})\pi]}{(\pi m)^{1/2}(\cos\alpha)^{l_1+1}(\sin\alpha)^{l_2+1}}. \tag{A8}$$

The diagonalization of each submatrix of $\underline{C}$ gives then eigenvalues c^{λ}_{ν} and eigenvectors $a^{\lambda}_{\eta,\nu}$. As mentioned above, only the lowest eigenstates are retained in each λ subspace. In the actual calculation, the lowest four eigenstates are retained up to $\lambda=41$ (this comes from the fact that for low λ's, the third and fourth eigenstate contributes to the second-lowest potential curve, the + channel in the $^1P^o$ symmetry). The lowest two were then used from $\lambda=43$ to 59, and the lowest one from $\lambda=59$ to 71, when an odd parity was being studied. Instead when an even parity was being studied, the lowest three such eigenstates were used up to $\lambda=66$.

These eigenstates were then used as a basis to finally diagonalize $\hat{U}$, so that the matrix elements are given by

$$U_{\lambda\nu,\lambda'\nu'}=\sum_{\eta,\eta'}\left[\frac{1}{R}a^{\lambda}_{\eta\nu}a^{\lambda'}_{\eta'\nu'}\langle\eta\,|\,C\,|\,\eta'\rangle\right]$$
$$+\frac{1}{R^2}[(\lambda+2)^2-\tfrac{1}{4}]\delta_{\lambda\lambda'}\delta_{\nu\nu'}. \tag{A9}$$

The diagonalization determines eigenvalues U_μ and their corresponding eigenvectors $z_{\lambda\nu,\mu}$.

APPENDIX B: COMPUTATION OF THE BODY-FRAME PROBABILITY DENSITY

In this appendix a method for calculating the density as a function of the angular variables α and θ_{12} is presented. In order to have a density independent of the space-fixed coordinate system, I calculate the scalar quantity $\rho_L^\mu(R;\alpha,\theta_{12})$:

$$\rho_L^\mu(R;\alpha,\theta_{12})=\sum_M |\Psi_{LM}^\mu|^2 . \tag{B1}$$

In order to do so, the wave function at any particular R value is written as

$$\Psi_{LM}^\mu=\sum_{l_1,l_2} G_{l_1 l_2}^\mu(\alpha) Y_{l_1 l_2 LM}(\hat{\mathbf{r}}_1,\hat{\mathbf{r}}_2) , \tag{B2}$$

where

$$G_{l_1 l_2}^\mu(\alpha) = \sum_{\lambda,\nu} N_{m l_1 l_2} z_{\lambda\nu,\mu} a_{\eta\nu}^\lambda (\cos\alpha)^{l_1+1}(\sin\alpha)^{l_2+1} \times F(-m,m+l_1+l_2+2,l_2+\tfrac{3}{2};\sin^2\alpha)\chi_{SM_S} , \tag{B3}$$

so that

$$\rho_L^\mu(\alpha,\theta_{12})=\sum_{\substack{l_1,l_2,\\ l_1',l_2',\\ M}} G_{l_1 l_2}^\mu(\alpha) G_{l_1' l_2'}^\mu(\alpha) Y_{l_1 l_2 LM}(\hat{\mathbf{r}}_1,\hat{\mathbf{r}}_2) \times Y_{l_1' l_2' LM}^*(\hat{\mathbf{r}}_1,\hat{\mathbf{r}}_2) . \tag{B4}$$

This expression can then be simplified into the form

$$\rho_L^\mu(R;\alpha,\theta_{12})=\sum_{\substack{l_1,l_2,\\ l_1',l_2',\\ k}} (-1)^{L+k}\frac{(2L+1)(2k+1)}{(4\pi)^2}[(2l_1+1)(2l_2+1)(2l_1'+1)(2l_2'+1)]^{1/2} \times G_{l_1 l_2}^\mu(\alpha) G_{l_1' l_2'}^\mu(\alpha) \begin{Bmatrix} l_1 & l_2 & L \\ l_2' & l_1' & k \end{Bmatrix} \begin{bmatrix} l_1 & l_1' & k \\ 0 & 0 & 0 \end{bmatrix} \begin{bmatrix} l_2' & l_2 & k \\ 0 & 0 & 0 \end{bmatrix} P_k(\cos\theta_{12}) . \tag{B5}$$

*Present address: Fakultät für Physik, Universität Freiburg, Hermann-Herder-Strasse 3, D-7800 Freiburg, West Germany. Permanent address: Escuela Colombiana de Ingenieria, A.A. 14520, Bogota, Columbia.

[1] J. A. Wheeler, Ann. N.Y. Acad. Sci. **48**, 219 (1946).

[2] A. P. Mills, Jr., Phys. Rev. Lett. **46**, 717 (1981).

[3] A. P. Mills, Jr., Phys. Rev. Lett. **50**, 617 (1983).

[4] J. Botero, Ph.D. dissertation, Louisiana State University, 1986. Available through University Microfilms International, 300 North Zeeb Road, Ann Arbor, MI 48106.

[5] E. A. Hylleraas, Phys. Rev. **71**, 491 (1949); A. A. Frost, M. Inokuti, and J. P. Lowe, J. Chem. Phys. **41**, 482 (1964); P. Cavaliere, G. Ferrante, R. Geracitano, and L. Lo Cascio, *ibid.* **63**, 624 (1975); Y. K. Ho, Phys. Rev. A **19**, 2347 (1979).

[6] J. Botero and C. H. Greene, Phys. Rev. A **32**, 1249 (1985). There is a misprint in this paper: Eq. (13) should read $\phi_{nl}=\mathcal{A} r_1 R_{nl}(r_a) r_2 r_b^{l+1} P_l(\hat{\mathbf{r}}_a\cdot\hat{\mathbf{r}}_b)$.

[7] J. Botero and C. H. Greene, Phys. Rev. Lett. **56**, 1366 (1986).

[8] C. H. Greene (private communication).

[9] H. E. Bethe and E. E. Salpeter, *Quantum Mechanics of One- and Two-Electron Atoms,* 1st ed. (Plenum, New York, 1977), p. 166.

[10] V. Fock, K. Nor. Vidensk. Selsksk. Forh. **31**, 138 (1958).

[11] J. M. Feagin and J. H. Macek, Phys. Rev. **32**, 3219 (1985).

[12] G. H. Wannier, Phys. Rev. **90**, 817 (1953).

[13] J. H. Macek, J. Phys. B **1**, 831 (1968).

[14] U. Fano, Rep. Prog. Phys. **46**, 97 (1983).

[15] C. D. Lin, Adv. At. Mol. Phys. (to be published).

[16] C. H. Greene, Phys. Rev. A **26**, 2974 (1982).

[17] U. Fano, Phys. Rev. A **24**, 2402 (1981).

[18] B. L. Christensen-Dalsgaard, Phys. Rev. A **29**, 470 (1984).

[19] C. H. Greene, Phys. Rev. A **23**, 661 (1981).

[20] C. D. Lin, Phys. Rev. A **12**, 493 (1975).

[21] A. R. P. Rau (private communication).

[22] K. Stefanski and H. S. Taylor, Phys. Rev. A **31**, 2810 (1985).

[23] D. Wintgen and H. Friedrich, J. Phys. B **19**, 991 (1986).

[24] M. J. Seaton, Proc. Phys. Soc. London **77**, 174 (1961).

[25] M. Gailitis and R. J. Damburg, Proc. Phys. Soc. London **82**, 192 (1963).

[26] A. F. Starace and G. L. Webster, Phys. Rev. A **19**, 1638 (1980).

[27] A. K. Bhatia and R. Drachman, Phys. Rev. A **28**, 2523 (1983).

[28] Y. K. Ho, J. Phys. B **16**, 1503 (1984).

[29] C. D. Lin, Phys. Rev. Lett. **35**, 1150 (1975).

[30] H. Klar and M. Klar, J. Phys. B **13**, 1057 (1980); M. Klar, Ph.D. Thesis, University of Freiburg, 1977.

[31] J. W. Cooper, U. Fano, and F. Prats, Phys. Rev. Lett. **10**, 518 (1963).

[32] L. D. Landau and E. M. Lifshitz, *Quantum Mechanics (Non-relativistic Theory),* 3rd ed. (Pergamon, New York, 1977), p. 300.

[33] A. P. Mills, Jr., Phys. Rev. A **24**, 3242 (1981).

[34] D. R. Herrick, M. E. Kellman, and R. D. Poliak, Phys. Rev. A **22**, 1517 (1980).

[35] U. Fano, Phys. Rev. **135**, B863 (1964), see also J. Botero, Ref. 4.

[36] S. J. Ward, J. W. Humberston, and M. R. C. McDowell, J. Phys. B **18**, L525 (1985); Europhys. Lett. **1** (4), 167 (1986); (unpublished).

[37] K. P. Arnold, F. Chunely, M. Eckhause, M. Gladisch, V. W. Hughes, J. Kane, S. Kettell, Y. Kuang, K. Kumar, D. Lu, B.

Ni, B. Mathias, H. Orth, R. Schaefer, P. Souder, K. Woodle, and G. zu Putlitz, presented in the 1986 Annual Joint American Physical Society/American Association of Physics Teachers Meeting in Atlanta, GA (unpublished).
[38]J. Botero (unpublished).
[39]I. I. Sobel'man, *Introduction to the Theory of Atomic Spectra,* 1st ed. (Pergamon, New York, 1972), p. 86.
[40]H. Bateman, *Higher Transcendental Functions,* 1st ed. (McGraw-Hill, New York, 1953), Vol. 2, p. 170, Eq. 16.
[41]H. Bateman, Ref. 40, p. 198, Eq. 10.
[42]H. A. Bethe and E. E. Salpeter, Ref. 9, p. 167.
[43]G. J. Schulz, Rev. Mod. Phys. **45**, 376 (1973).
[44]J. Callaway, Phys. Lett. **45A**, 315 (1978).